NANO LETTERS

Letter

pubs.acs.org/NanoLett

Facet Energy and Reactivity versus Cytotoxicity: The Surprising Behavior of CdS Nanorods

Lu Liu,[*,†] Meiqing Sun,[†] Haijun Zhang,[†] Qilin Yu,[‡] Mingchun Li,[‡] Yu Qi,[†] Chengdong Zhang,[†] Guandao Gao,[†] Yingjin Yuan,[§] Huanhuan Zhai,[∥] Wei Chen,[*,†] and Pedro J. J. Alvarez[*,⊥]

[†]Tianjin Key Laboratory of Environmental Remediation and Pollution Control, College of Environmental Science and Engineering, Nankai University, Wei Jin Rd. 94, Tianjin 300071, China

[‡]Ministry of Education Key Laboratory of Molecular Microbiology and Technology, College of Life Science, Nankai University, Wei Jin Rd. 94, Tianjin 300071, China

[§]Ministry of Education Key Laboratory of Systems Bioengineering, Tianjin University, Wei Jin Rd. 92, Tianjin 300072, China

[∥]Tianjin Institute of Industrial Biotechnology, Chinese Academy of Sciences, Airport Economic Zone, Seven West Rd. 32, Tianjin 300308, China

[⊥]Department of Civil and Environmental Engineering, Rice University, 6100 Main Street, Houston, Texas 77005, United States

Supporting Information

ABSTRACT: Responsible development of nanotechnology calls for improved understanding of how nanomaterial surface energy and reactivity affect potential toxicity. Here, we challenge the paradigm that cytotoxicity increases with nanoparticle reactivity. Higher-surface-energy {001}-faceted CdS nanorods (CdS-H) were less toxic to *Saccharomyces cerevisiae* than lower-energy ({101}-faceted) nanorods (CdS-L) of similar morphology, aggregate size, and charge. CdS-H adsorbed to the yeast's cell wall to a greater extent than CdS-L, which decreased endocytosis and cytotoxicity. Higher uptake of CdS-L decreased cell viability and increased endoplasmatic reticulum stress despite lower release of toxic Cd^{2+} ions. Higher toxicity of CdS-L was confirmed with five different unicellular microorganisms. Overall, higher-energy nanocrystals may exhibit greater propensity to adsorb to or react with biological protective barriers and/or background constituents, which passivates their reactivity and reduces their bioavailability and cytotoxicity.

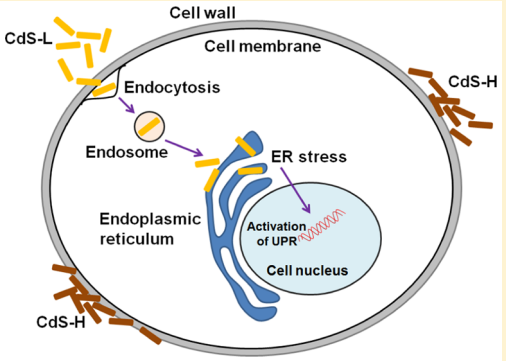

KEYWORDS: *Surface energy, crystal facets, nanotoxicity, CdS nanorods, Saccharomyces cerevisiae*

Nanomaterials offer great promise to enhance many areas of applications such as electronics, catalysis, and biomedicine.[1−10] With the increasing production and use of nanomaterials, their potential toxicity has received much attention.[11−19] The reactivity and toxicity of nanomaterials are largely dependent on their physicochemical properties. A number of studies have addressed the effects of nanoparticle size, shape, elemental composition, surface functionalization and modification, and crystalline structure on toxicity.[20,21] Such properties can affect nanomaterials tendency to aggregate, migrate, adsorb, release toxic metal ions, or react with various environmental or biological constituents, and, consequently, affect their bioavailability, cellular uptake, and cytotoxicity.[22−26] Yet, nanomaterial surface structure−toxicity relationships are poorly understood.

Crystalline nanomaterials (e.g., metals, metal oxides, and other metal-based nanomaterials) with different exposed crystal facets possess different surface energies and thus may exhibit markedly varied reactivity in aqueous solutions.[4,27−31] For example, the electrochemical catalytic activity of Ag_3PO_4 with exposed {111} facets was 10-fold higher than that of Ag_3PO_4 with exposed {100} or {110} facets.[4] It is therefore reasonable to expect that the surface energy and reactivity of the exposed facets of a nanocrystal can also greatly affect its toxicity.

To date, only one article has considered the facet-dependent toxicity of crystals.[32] This study reported higher antibacterial activity of Cu_2O octahedral crystals bounded by {111} facets than cubic crystals bounded by {100} facets and attributed this facet-dependent difference to the atomic arrangement of the exposed surfaces. Yet, no previous publications have compared the facet-dependent toxicity of nanocrystals of similar morphology and aggregate size, which is important to assess whether facet energy is an important determinant of cytotoxicity.

Herein we investigate the facet-dependent cytotoxicity of two hexagonal CdS nanorods with similar physical dimensions but

Received: November 4, 2015
Revised: December 11, 2015
Published: December 17, 2015

DOI: 10.1021/acs.nanolett.5b04487
Nano Lett. 2016, 16, 688−694

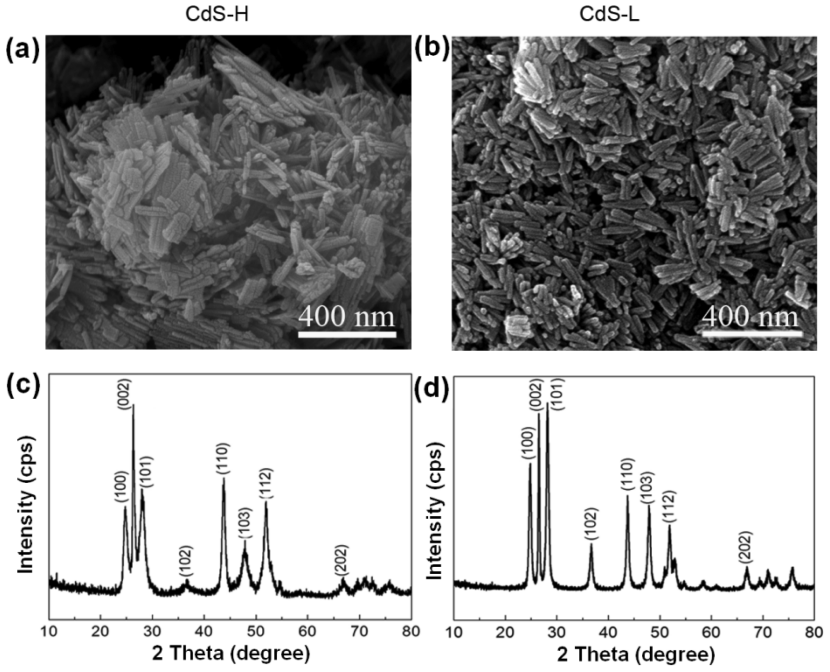

Figure 1. Scanning electron microscopy images (a,b) and X-ray diffraction patterns (c,d) of CdS-H and CdS-L.

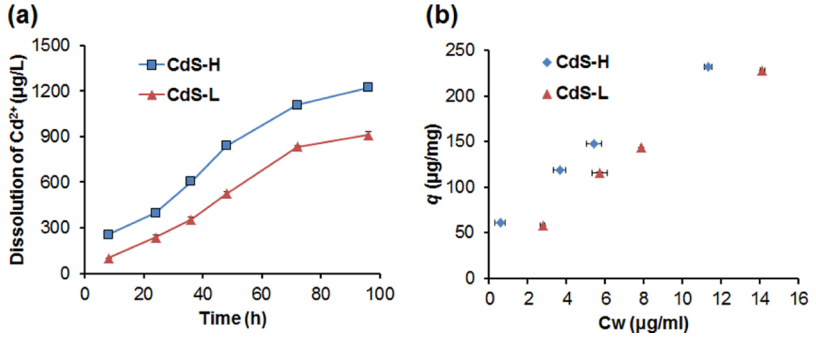

Figure 2. Higher reactivity of CdS-H than CdS-L (640 mg/L). (a) Higher Cd^{2+} release in YPD medium. (b) Higher affinity to bovine serum albumin (a model protein) is illustrated by adsorption isotherms in deionized water, which depict the concentrations of bovine serum albumin on CdS (q) versus concentrations in deionized water (C_w).

different exposed facets: higher-surface-energy {001}-faceted CdS nanorods (CdS-H) versus a lower-surface-energy {101}-faceted nanorods (CdS-L). We chose the yeast *Saccharomyces cerevisiae* as a test organism because it is the most intensively studied unicellular eukaryotic fungus and its cellular structure and functional organization have many similarities with cells of higher level organisms.[33] Even though the higher-energy CdS-H released more toxic Cd^{2+} ions, it was less cytotoxic. The results were corroborated by toxicity assays with five different unicellular organisms: the fungi *Rhizopus niger*, *Cryptococcus neoformans*, and *Candida albicans*, and the bacteria *Escherichia coli* and *Staphylococcus aureus*. We attribute the surprisingly lower toxicity of the higher-energy CdS-H to its higher reactivity with biological protective barriers and/or background constituents that passivate nanoparticle reactivity or reduce bioavailability. Specifically, CdS-H bound to the yeast's cell wall to a greater extent than CdS-L, which decreased endocytosis and cytotoxicity. This represents a caveat against generalizations of the relationship between nanoparticle reactivity and toxicity.

CdS Nanorods with Exposed {001} Facets (CdS-H) Have Similar Morphology, Aggregate Size, and Charge to Those with {101} Facets (CdS-L). Selected physicochemical characteristics of CdS-H and CdS-L are compared in Supporting Information (SI) Table S1. Both CdS nanocrystals have similar rod-like morphology: CdS-H is approximately 25 nm in diameter and 110 nm in length, and CdS-L is approximately 22 nm in diameter and 108 nm in length (Figure 1a,b; Figure S1a,b). The X-ray diffraction patterns (Figure 1c,d) show that CdS-H and CdS-L have the strongest {002} and {101} peaks, respectively, indicating the corresponding preferred orientations along the {002} and {101} planes. High resolution transmission electron microscopy images (SI Figure S1) show that the fringe spacings of 0.180 nm (CdS-H) and 0.304 nm (CdS-L) agree with the values of the {200} and {010} lattice planes (0.179 and 0.301 nm) of hexagonal-structure CdS. Accordingly, the CdS samples had dominantly exposed {002} and {101} surfaces, which are perpendicular to the {200} and {010} planes, respectively. Note that the {001} facets (that were used in the calculation of surface energy) are parallel to the {002} facets.

Because aggregation may affect the bioavailability and uptake of nanoparticles,[34] we compared the aggregate properties of CdS-H and CdS-L in the exposure medium (YPD, 1% yeast

DOI: 10.1021/acs.nanolett.5b04487
Nano Lett. 2016, 16, 688−694

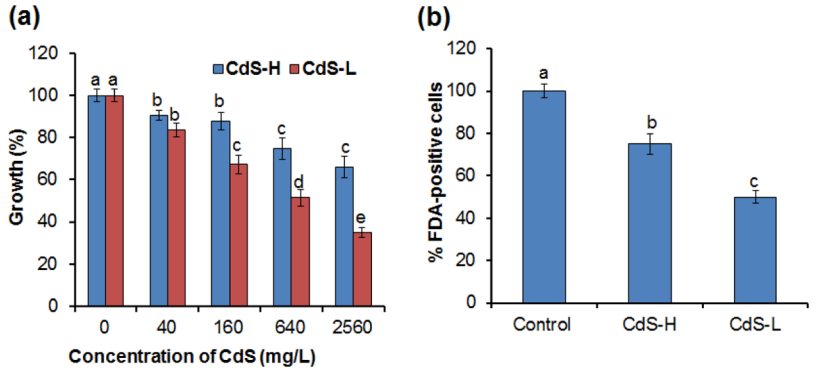

Figure 3. Higher toxicity of CdS-L than CdS-H to *S. cerevisiae* in YPD medium. (a) Growth inhibition (24 h exposure). (b) Cell viability assessed by FDA assay of esterase activity in the presence of 640 mg/L of CdS-H or CdS-L for 6 h. At least 20 fields were counted (see Supplementary Figure S6 for typical images). Values represent means ± one standard deviation. Identical letters indicate no statistical differences among treatments ($P > 0.05$). "Control" represents sample receiving no Cd treatment.

extract, 2% peptone, 2% dextrose). Different methods to measure nanoparticle sizes are known to yield different results due to inherent biases, such as stronger light scattering of larger particles for dynamic light scattering (DLS) and aggregation during sample preparation for microscopy.[35] Nevertheless, DLS showed similar aggregate sizes for the two nanorod suspensions (hydrodynamic diameters of 752 ± 170 nm for CdS-H versus 718 ± 158 nm for CdS-L) (Figure S2a), which was corroborated by optical microscopy (360 ± 187 for CdS-H versus 470 ± 182 for CdS-L) (Figure S3). Aggregation kinetics were also very similar for CdS-H and CdS-L (Figure S2b). Transmission electron microscopy images show that both CdS-H and CdS-L dispersed relatively well in YPD medium, forming loose clusters but not tightly packed aggregates (Figure S4). Finally, both CdS-H and CdS-L were negatively charged in the exposure medium, with similar zeta potential values (ζ) of −12.3 and −9.92 mV, respectively. Overall, these analyses show that potential differences in aggregate size and charge were not a confounding factor in cytotoxicity assays.

CdS-H Has Higher Surface Energy than CdS-L. The surface energy of the CdS nanorods was calculated based on the slab models (SI Figure S5), using the density functional theory approach.[27] The calculated surface energy of the {001} facets of CdS crystal was 0.627 J/m^2, whereas that of the {101} facets was 0.451 J/m^2. Consistent with its higher surface energy, CdS-H was able to release a greater amount of Cd^{2+} than CdS-L (Figure 2a). Additionally, consistent with the higher surface energy of CdS-H, it exhibited a greater adsorption affinity for a model protein, bovine serum albumin, than CdS-L (Figure 2b). The {001} facets possess higher density of unsaturated Cd atoms,[36] resulting in greater adsorption affinity of CdS-H for proteins (and biological constituents of similar structures) through specific chemical bindings,[37,38] possibly between exposed Cd ions and sulfur-containing moieties of proteins.[39] Thus, CdS-H would be more reactive (and bind) with background constituents or biological protective barriers than CdS-L.

CdS-H Is Less Cytotoxic than CdS-L. Even though the higher-energy CdS-H released a greater amount of Cd^{2+}, CdS-H was significantly less toxic than CdS-L (Figure 3a). For example, at an exposure concentration of 640 mg/L, CdS-L resulted in 48% inhibition of cell growth, whereas CdS-H caused only 25% growth inhibition. The different effects of CdS-H and CdS-L on cell viability are also evident based on the fluorescence diacetate (FDA) staining data (SI Figure S6). Living cells have esterase activity, causing the transformation of nonfluorescent FDA to fluorescent fluorescein, whereas dead cells have no esterase activity and cannot generate the fluorescent product.[40] Figure S6 shows more viable cells for CdS-H-treated cells, corroborating the lower toxicity of CdS-H. A comparison of cell viability between CdS-H and CdS-L treated samples is given in Figure 3b. Consistent with these results, CdS-L also exhibited higher growth inhibition than CdS-H to three different fungi (i.e., *Rhizopus niger*, *Cryptococcus neoformans*, and *Candida albicans*) and two bacteria (i.e., *Escherichia coli* and *Staphylococcus aureus*) (SI Figure S7), even though specific toxicity and defense mechanisms may vary from one species to another.

Lower Endocytosis Potential of CdS-H Contributes to Its Lower Toxicity. The lower toxicity of CdS-H than CdS-L deviates from common reports that the more reactive nanomaterials (including those that release more metal ions) exert higher toxicity.[41−44] To understand the difference in toxicity, we compared the endocytosis potential between CdS-H and CdS-L because it has been proposed that nanoparticle internalization plays an important role in cytotoxicity.[45−48] For *Saccharomyces cerevisiae*, the total amount of cell-associated Cd (including sorption and intracellular accumulation) was approximately twice higher for CdS-L than for CdS-H (Figure 4). Interestingly, the intracellular Cd content of CdS-H only accounted for a small fraction (<15%) of the total cell-associated Cd. In contrast, the intracellular Cd content of cells exposed to CdS-L accounted for a large fraction (~70%) of the total cell-associated Cd. Apparently, the difference in endocytosis potential played a critical role in the facet-dependent toxicity of the two CdS nanorods: the lower-surface-energy CdS nanorods were more easily internalized and exerted greater toxicity.

To further assess the role of endocytosis, we repeated these experiments with the *S. cerevisiae end3*Δ mutant, in which the gene *END3* essential for endocytosis was deleted. Interestingly, for CdS-H, the total amount of cell-associated Cd was statistically indistinguishable for the mutant and wild-type cells (Figure 4), indicating that endocytosis is a minor Cd accumulation mechanism for CdS-H. In contrast, endocytosis is very important for CdS-L accumulation, as shown by significantly lower ($p < 0.05$) total Cd accumulation by endocytosis-deficient mutant cells. To further confirm the difference in endocytosis potential between CdS-H and CdS-L, we examined the endocytic structures in CdS-treated cells by

DOI: 10.1021/acs.nanolett.5b04487
Nano Lett. 2016, 16, 688−694

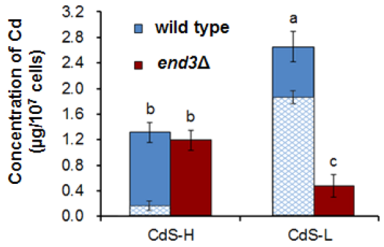

Figure 4. Total Cd accumulation in wild-type versus endocytosis-deficient mutant (*end3*Δ) *Saccharomyces cerevisiae* exposed to 640 mg/L CdS-H or CdS-L for 24 h. No difference was observed for CdS-H between wild-type and *end3*Δ, with Cd accumulation primarily in cell wall. In contrast, significantly higher Cd accumulation due to endocytosis was observed for wild-type exposed to CdS-L. Note that *end3*Δ accumulated less Cd when exposed to CdS-L than CdS-H, due to the higher affinity of the latter for cell wall constituents. The checked patterns represent the portion of the total Cd accumulation that occurred intracellularly. The error bars indicate standard deviations (n = 3). Identical letters indicate no statistically significant differences between treatments (P > 0.05).

the lipophilic styryl dye, *N*-(3- triethylammoniumpropyl)-4-(*p*-diethylaminophenyl-hexatrienyl) pyridinium dibromide (FM4-64). As shown in SI Figure S8, abundant endosomes (indicated by the white arrows) were observed near the cell wall in CdS-L treated cells, indicating a strong endocytosis activity. However, very few endosomes were observed in the control sample and the CdS-H treated cells.

Because nanoparticle-induced damage of cell membranes has also been recognized as an important mechanism for nanotoxicity,[41] we compared the effects of CdS-H and CdS-L on the integrity of cell membranes using propidium iodide (PI) intracellular (DNA) staining. Very few PI-positive cells were observed under the treatment of both CdS-H and CdS-L (SI Figure S9), suggesting no significant disruption of cell membranes by either CdS-H or CdS-L.

Binding of CdS-H to Cell Wall Inhibits Its Endocytosis. Unlike CdS-L, CdS-H aggregates of similar size (Figures S2–S4) and surface charge (Table S1) could not be readily endocytosed. Apparently, the more reactive CdS-H was bound to the cell wall to a greater extent than CdS-L, which corroborates the observed higher sorption affinity of CdS-H for the model protein (Figure 2b). High angle annular dark field image scanning transmission electron microscopy shows that CdS-H accumulated mainly on the cell wall, whereas CdS-L was observed inside cells (Figure 5). Particles that are bound to the cell wall are less bioavailable for endocytosis, which requires that the particles penetrate further to reach the plasma membrane.[49,50] Whether the uptake of CdS-H was also hindered by its binding to structural or regulatory proteins involved in endocytosis or by causing other physiological damage remains to be determined, although no membrane damage was detected (Figure S9).

Interestingly, the accumulation of CdS-H in the *end3*Δ mutant was significantly greater than that of CdS-L (Figure 4). Because the *end3*Δ mutant cannot readily internalize CdS nanorods, the measured Cd accumulation can be mainly attributed to CdS associated with cell walls. This conclusion is supported by the transmission electron microscopy images and energy dispersive spectrometry analysis (SI Figures S10 and S11), which show that CdS nanorods and Cd element were not detected inside *end3*Δ mutant cells treated with CdS-H or CdS-L. The substantial difference in Cd content confirms the stronger binding of CdS-H to cell walls. These results do not rule out the possibility that some higher-surface-energy nanoparticles also react with and get passivated by constituents of the extracellular environment, acquiring coatings that affect their uptake and toxicity potential. Nevertheless, particle morphology and aggregate properties (size, surface area, and charge) were statistically indistinguishable between CdS-H and CdS-L (Table S1), underscoring that differences in surface energy were a critical determinant of differences in cytotoxicity.

Additional experiments were conducted to determine the effect of surface passivation on nanoparticle bioavailability and intracellular uptake. These endocytosis experiments were conducted with CdS-H and CdS-L that had been similarly coated with polyethylene glycol (PEG) (Figure S12). PEG forms an inert layer for bioadsorption, which provides similar conditions for endocytosis and minimizes the potential effects of extracellular nanoparticle interactions.[51,52] Accordingly, unlike uncoated nanorods, uptake of PEG-coated CdS-H and CdS-L was statistically indistinguishable (Figure S13). Furthermore, the PEG-coated CdS-H was internalized to a significantly higher extent than the corresponding uncoated

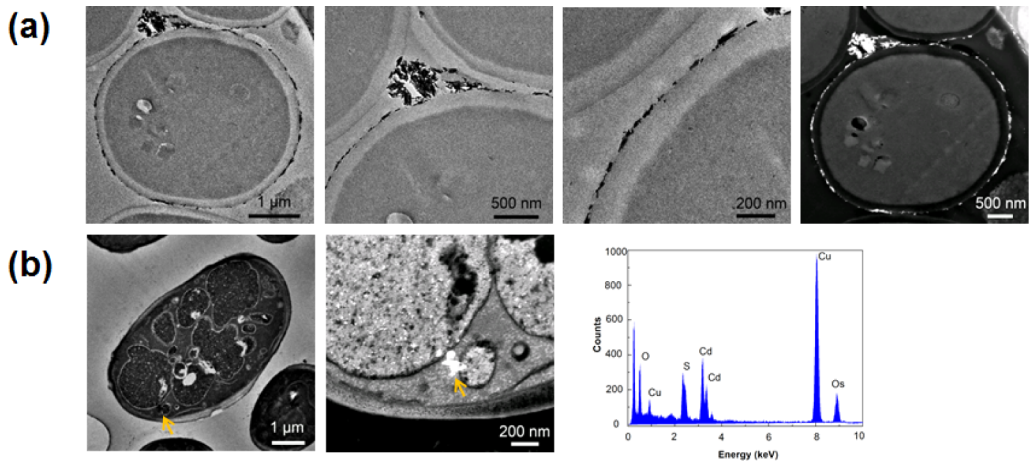

Figure 5. Distribution of CdS nanorods with different facets in yeast cells. (a) Accumulation of CdS-H on cell wall. (b) Intracellular uptake of CdS-L by *Saccharomyces cerevisiae*. Cells were exposed to 640 mg/L CdS-L for 24 h. Accumulation of CdS-L in the cytoplasm was confirmed by energy-dispersive X-ray spectroscopy (bottom right panel).

DOI: 10.1021/acs.nanolett.5b04487
Nano Lett. 2016, 16, 688–694

(unpassivated) nanorods (Figure S13). This corroborates that higher-surface-energy (uncoated) nanoparticles exhibit greater propensity to adsorb to or react with biological protective barriers, which reduces their bioavailability and uptake potential.

Greater Endocytosis Potential of CdS-L Results in Activation of Endoplasmic Reticulum (ER) Stress. We postulate that the higher toxicity of CdS-L than CdS-H was caused primarily by higher ER stress resulting from a higher extent of internalization. The ER plays important roles in cell normal survival, such as protein synthesis, folding, modification, and transport, and ER stress can result in accumulation of misfolded proteins, which leads to apoptosis and/or necrosis.[53−55] To test this hypothesis, we evaluated ER stress using the reporter plasmid pJC104, whose expression levels can be used to characterize ER stress.[56] Consistent with this hypothesis, the β-galactosidase assays showed that both CdS-H and CdS-L increased the expression of unfolded protein response (UPR) promoter-governed *LacZ* gene, indicating that ER stress was exerted by both materials (Figure 6). The effect

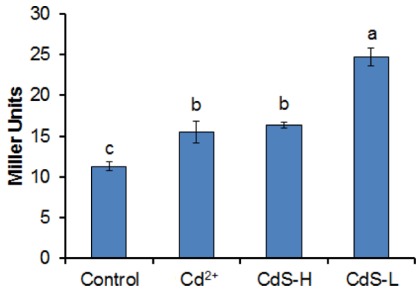

Figure 6. Higher endoplasmic reticulum (ER) stress exerted by CdS-L than CdS-H (640 mg/L each) and Cd^{2+} (0.4 mg/L, representing maximum released concentration) after 6 h exposure. ER stress was measured by pJC104 expression levels in yeast cells. The error bars indicate one standard deviations (n = 3). Identical letters indicate no statistical differences among treatments (P > 0.05). "Control" represents sample receiving no Cd treatment.

of CdS-H was statistically indistinguishable from that of Cd^{2+}, whereas CdS-L showed much stronger activity in up-regulating *LacZ* expression, indicating that CdS-L can cause much more severe ER stress than CdS-H, which leads to cell death.

In summary, more reactive {001}-faceted CdS nanorods (CdS-H) were less toxic to several monocellular organisms than lower-surface-energy {101}-faceted nanorods (CdS-L) of similar morphology, aggregate size, and charge, even though CdS-H released a greater amount of toxic Cd^{2+}. For *Saccharomyces cerevisiae*, the lower toxicity of higher-energy CdS-H is attributable to its stronger binding to the yeast's cell wall, which decreased endocytosis and cytotoxicity. In contrast, higher uptake of CdS-L resulted in higher cytotoxicity (i.e., decreased cell viability, higher endoplasmatic reticulum stress, and hindered growth). This represents a caveat against the current paradigm that more reactive nanoparticles are more cytotoxic and underscores the need for further studies with a broader range of nanocrystals to determine whether higher-energy facets are more prone to passivating reactions in the environment that decrease their bioavailability and attenuate their potential impact.

Methods. *Synthesis and Characterization of CdS Nanorods.* The two CdS nanorods were synthesized using a hydrothermal method. To synthesize the CdS nanorods with the {001} facets, 0.3 g of $CdCl_2$ and 0.4 g of thiourea were added to a Teflon-lined stainless steel autoclave of 30 mL capacity. Then, 2 mL of distilled water and 18 mL of ethylenediamine were added. The autoclave was heated in an oven at 150 °C for 5 h, and then allowed to cool to room temperature. The yellowish product was collected and washed with distilled water and ethanol. The CdS nanorods with the {101} facets were synthesized using a method modified from that of Xiong et al.[57] Additional experiments were conducted with nanorods coated with polyethylene glycol (24 h exposure to PEG 3350, Sigma-Aldrich) to assess the impact of surface passivation on nanoparticle bioavailability and cellular uptake. The detailed procedures are given in SI section 7.

The surface energy of the {001} and {101} facets of CdS crystal were computed through density functional theory, and the computational details are given in SI. The CdS nanorods were characterized with X-ray diffraction (XRD, D/MAX2500, JAPAN SCIENCE) with Cu Ka radiation (λ = 1.54056 Å), field-emission scanning electron microscopy (FE-SEM, Nanosem 430, FEI), and high-resolution transmission electron microscopy (HRTEM, Tecnai G^2 F-20, FEI, operating voltage of 200 kV). Aggregation properties of CdS nanorods in exposure medium (YPD medium) were characterized with transmission electron microscopy (TEM, Tecnai G^2 F-20, FEI). The hydrodynamic diameters and aggregation kinetics in YPD medium were determined using a ZetaSizer (Malvern). Particle size distribution in YPD medium was also obtained based on optical microscopy images (Leica DM3000) using ImageJ (National Institutes of Health).

Dissolution and Adsorption Experiments. To evaluate the release of Cd^{2+} from CdS, 3 mL of cell suspension was mixed with 3 mL of diluted CdS suspension, to give a CdS concentration of 640 mg/L. The mixture was shaken at 180 rpm and 30 °C. At predetermined time intervals the mixture was centrifuged at 12,000 rpm for 30 min.[58] The supernatant was collected and digested with 30% HNO_3, and the total Cd concentration was determined with inductively coupled plasma−mass spectrometry (ICP−MS, PerkinElmer, ELAN DRC-e). Adsorption isotherms of bovine serum albumin to CdS-H and CdS-L were obtained using a previously developed method.[59] The detailed procedures are described in SI.

Yeast Strains and Growth Conditions. The wild-type *S. cerevisiae* strain INVSc1 was obtained from Invitrogen. The endocytic deficient mutant *end3*Δ was obtained from Prof. Yingjin Yuan, Tianjin University. Yeast cells from single colonies were cultured by shaking at 30 °C in liquid YPD medium overnight before use.

Growth Inhibition and Cell Viability Assays. Cell growth was determined by direct cell number counting using a hemocytometer. Briefly, 1 mL of cell suspension was mixed with 1 mL of diluted CdS suspension, to give a CdS concentration of 40, 160, 640, and 2560 mg/L, respectively. The mixtures were cultured at 30 °C by shaking at 180 rpm for 24 h. Cell viability was determined by FDA staining after 6 h of treatment,[60] and the detailed methods are described in SI.

Particle Uptake Measurement. To determine the total amounts of Cd adhering to and inside yeast cells, the cell media were removed after 24 h of incubation with CdS nanorods (640 mg/L) and washed five times with a phosphate buffer solution (PBS) to remove the nonadhered/internalized particles. The harvested cells were diluted to 1 mL. Next, 50 μL of the cells was diluted with 1 mL ddH_2O, and the optical density (OD) was measured to observed the cells numbers. The other 950 μL

DOI: 10.1021/acs.nanolett.5b04487
Nano Lett. 2016, 16, 688−694

was centrifuged, digested with 400 μL of HNO_3 overnight, and then diluted to a final volume of 10 mL with Milli-Q water. Afterward, the Cd content was determined with ICP−MS. To determine the mass of Cd inside the cells, the washed cells were treated with 100 U/mL snailase for 1 h to remove the cell walls, and the protoplasts were harvested by centrifugation. These cells were then digested with HNO_3 as described above, and the Cd contents were quantified.[48] The endocytic phenomena observation was described in SI.

TEM Analysis of Yeast Cells. After incubation with 640 mg/L of CdS for 24 h, the yeast cells were harvested, washed three times with PBS, and fixed with a 2% glutaraldehyde solution at 4 °C for 10 h, followed by postfixing for 2 h with 1% osmium tetroxide solution. The samples were dehydrated with graded ethanol, and then infiltrated and embedded in Spurr's resin. Thin sections stained with (U) were mounted on copper grids and then observed on transmission electron microscopy (TEM, Tecnai G^2 F-20, FEI). Next, EDS (Axis Ultra DLD, Kratos) was used to identify the elements, such as Cd or S.

ER Stress Assay. The yeast strain was transformed with the UPR reporting plasmids pJC104, which contains the reporter gene *LacZ* (encoding β-galactosidase) under the control of 4 × UPRE.[56,61] β-Galactosidase assays were conducted using the method of Yu et al.[62]

Statistical Analysis. Statistical significance in the differences was evaluated by Student's *t* tests or Tukey's method after analysis of variance (ANOVA).

■ ASSOCIATED CONTENT

Supporting Information

The Supporting Information is available free of charge on the ACS Publications website at DOI: 10.1021/acs.nanolett.5b04487.

Material synthesis, density functional theory (DFT) computations, toxicity tests with *R. niger*, *C. neoformans*, *C. albicans*, *E. coli*, and *S. aureus*, nanorod adsorption experiments, cell viability, assays, endocytocis data, and additional experiments with PEG-coated nanorods to determine the impact of surface passivation on nanoparticle bioavailability (PDF)

■ AUTHOR INFORMATION

Corresponding Authors

*E-mail: alvarez@rice.edu. Fax: (713) 348 5268.
*E-mail: liul@nankai.edu.cn.
*E-mail: chenwei@nankai.edu.cn.

Author Contributions

L.L., W.C., and P.A. designed the study and wrote the manuscript. M.S. and Q.Y. performed the experiments. H.Z. performed theoretical calculations of surface energy. M.L. provided microbiology experiment platform. C.Z. and G.G. gave experimental guidance. Y.Y. provided endocytic deficient mutant *end3*Δ. H.Z. performed transmission electron microscopy of yeast cells. All authors discussed the results and commented on the manuscript.

Notes

The authors declare no competing financial interest.

■ ACKNOWLEDGMENTS

This work was supported by the Ministry of Science and Technology of China (Grant 2014CB932001) and National Natural Science Foundation of China (Grants 21425729 and 21271108). Partial funding was provided by the NSF ERC on Nanotechnology-Enabled Water Treatment (EEC-1449500). We thank Professor David Levin (Boston University) for providing the plasmid p2052 and Professor Jeffery Cox (University of California, San Francisco) for providing the reporter plasmid pJC104.

■ REFERENCES

(1) Ke, S. H.; Yang, W.; Baranger, H. U. *Nano Lett.* **2008**, *8*, 3257−3261.
(2) Hwang, S. W.; Lee, C. H.; Cheng, H. Y.; Jeong, J. W.; Kang, S. K.; Kim, J. H.; Shin, J.; Yang, J.; Liu, Z. J.; Ameer, G. A.; Huang, Y. G.; Rogers, J. A. *Nano Lett.* **2015**, *15*, 2801−2808.
(3) Takahashi, T.; Takei, K.; Gillies, A. G.; Fearing, R. S.; Javey, A. *Nano Lett.* **2011**, *11*, 5408−5413.
(4) Martin, D. J.; Umezawa, N.; Chen, X. W.; Ye, J. H.; Tang, J. W. *Energy Environ. Sci.* **2013**, *6*, 3380−3386.
(5) Stolojan, V.; Tison, Y.; Chen, G. Y.; Silva, R. *Nano Lett.* **2006**, *6*, 1837−1841.
(6) Li, Y. M.; Somorjai, G. A. *Nano Lett.* **2010**, *10*, 2289−2295.
(7) Zhang, Q.; Shu, X. Z.; Lucas, J. M.; Toste, F. D.; Somorjai, G. A.; Alivisatos, A. P. *Nano Lett.* **2014**, *14*, 379−383.
(8) Peng, Z. M.; You, H. J.; Wu, J. B.; Yang, H. *Nano Lett.* **2010**, *10*, 1492−1496.
(9) Wei, H.; Insin, N.; Lee, J. M.; Han, H. S.; Cordero, J. M.; Liu, W. H.; Bawendi, M. G. *Nano Lett.* **2012**, *12*, 22−25.
(10) Zhang, J. F.; Li, Y. N.; An, F. F.; Zhang, X. H.; Chen, X. F.; Lee, C. S. *Nano Lett.* **2015**, *15*, 313−318.
(11) Lesniak, W.; Bielinska, A. U.; Sun, K.; Janczak, K. W.; Shi, X. Y.; BakerJr, J. R.; Balogh, L. P. *Nano Lett.* **2005**, *5*, 2123−2130.
(12) Derfus, A. M.; Chan, W. C. W.; Bhatia, S. N. *Nano Lett.* **2004**, *4*, 11−18.
(13) Qiao, R.; Roberts, A. P.; Mount, A. S.; Klaine, S. J.; Ke, P. C. *Nano Lett.* **2007**, *7*, 614−619.
(14) Morales, M. I.; Rico, C. M.; Hernandez-Viezcas, J. A.; Nunez, J. E.; Barrios, A. C.; Tafoya, A.; Flores-Marges, J. P.; Peralta-Videa, J. R.; Gardea-Torresdey, J. L. *J. Agric. Food Chem.* **2013**, *61*, 6224−6230.
(15) Tong, Z. H.; Bischoff, M.; Nies, L.; Applegate, B.; Turco, R. F. *Environ. Sci. Technol.* **2007**, *41*, 2985−2991.
(16) Rodrigues, D. F.; Jaisi, D. P.; Elimelech, M. *Environ. Sci. Technol.* **2012**, *47*, 625−633.
(17) Lyon, D. Y.; Brunet, L.; Hinkal, G. W.; Wiesner, M. R.; Alvarez, P. J. J. *Nano Lett.* **2008**, *8*, 1539−1543.
(18) Handy, R. D.; Cornelis, G.; Fernandes, T.; Tsyusko, O.; Decho, A.; Sabo-Attwood, T.; Metcalfe, C.; Steevens, J. A.; Klaine, S. J.; Koelmans, A. A.; Horne, N. *Environ. Toxicol. Chem.* **2012**, *31*, 15−31.
(19) Auffan, M.; Tella, M.; Santaella, C.; Brousset, L.; Pailles, C.; Barakat, M.; Espinasse, B.; Artells, E.; Issartel, J.; Issartel, J.; Masion, A.; Rose, J.; Wiesner, M. R.; Achouak, W.; Thiery, A.; Bottero, J. Y. *Sci. Rep.* **2014**, *4*, 1−7.
(20) Nagai, H.; Okazaki, Y.; Chew, S. H.; Misawa, N.; Yamashita, Y.; Akatsuka, S.; Ishihara, T.; Yamashita, K.; Yoshikawa, Y.; Yasui, H.; Jiang, L.; Ohara, H.; Takahashi, T.; Ichihara, G.; Kostarelos, K.; Miyata, Y.; Shinohara, H.; Toyokuni, S. *Proc. Natl. Acad. Sci. U. S. A.* **2011**, *108*, E1330−E1338.
(21) Fiorito, S.; Serafino, A.; Andreola, F.; Togna, A.; Togna, G. *J. Nanosci. Nanotechnol.* **2006**, *6*, 591−599.
(22) Qu, Y.; Li, W.; Zhou, Y. L.; Liu, X. F.; Zhang, L. L.; Wang, L. M.; Li, Y. F.; Iida, A.; Tang, Z. Y.; Zhao, Y. L.; Chai, Z. F.; Chen, C. Y. *Nano Lett.* **2011**, *11*, 3174−3183.
(23) Kagan, V. E.; Konduru, N. V.; Feng, W.; Allen, B. L.; Conroy, J.; Volkov, Y.; Vlasova, I. I.; Belikova, N. A.; Yanamala, N.; Kapralov, A.; Tyurina, Y. Y.; Shi, J.; Kisin, E. R.; Murray, A. R.; Franks, J.; Stolz, D.; Gou, P.; Klein-Seetharaman, J.; Fadeel, B.; Star, A.; Shvedova, A. A. *Nat. Nanotechnol.* **2010**, *5*, 354−359.
(24) Ye, L.; Yong, K. T.; Liu, L.; Roy, I.; Hu, R.; Zhu, J.; Cai, H.; Law, W. C.; Liu, J.; Wang, K.; Liu, J.; Liu, Y.; Hu, Y.; Zhang, X.; Swihart, M. T.; Prasad, P. N. *Nat. Nanotechnol.* **2012**, *7*, 453−458.

DOI: 10.1021/acs.nanolett.5b04487
Nano Lett. 2016, 16, 688−694

(25) Auffan, M.; Bertin, D.; Chaurand, P.; Pailles, C.; Dominici, C.; Rose, J.; Bottero, J. Y.; Thiery, A. *Water Res.* **2013**, *47*, 3921−3930.
(26) Artells, E.; Issartel, J.; Auffan, M.; Borschneck, D.; Thill, A.; Tella, M.; Brousset, L.; Rose, J.; Bottero, J. Y.; Thiery, A. *PLoS One* **2013**, *8*, e71260.
(27) Bi, Y. P.; Ouyang, S.; Umezawa, N.; Cao, J.; Ye, J. *J. Am. Chem. Soc.* **2011**, *133*, 6490−6492.
(28) Gong, X. Q.; Selloni, A.; Batzill, M.; Diebold, U. *Nat. Mater.* **2006**, *5*, 665−670.
(29) Fujishima, A.; Honda, K. *Nature* **1972**, *238*, 37−38.
(30) Zhao, K.; Zhang, L.; Wang, J.; Li, Q.; He, W.; Yin, J. J. *J. Am. Chem. Soc.* **2013**, *135*, 15750−15753.
(31) Ye, L.; Tian, L.; Peng, T.; Zan, L. *J. Mater. Chem.* **2011**, *21*, 12479−12484.
(32) Ren, J.; Wang, W.; Sun, S.; Zhang, L.; Wang, L.; Chang, J. *Ind. Eng. Chem. Res.* **2011**, *50*, 10366−10369.
(33) Kasemets, K.; Ivask, A.; Dubourguier, H. C.; Kahru, A. *Toxicol. In Vitro* **2009**, *23*, 1116−1122.
(34) Zhu, M. T.; Nie, G. J.; Meng, H.; Xia, T.; Nel, A.; Zhao, Y. L. *Acc. Chem. Res.* **2013**, *46*, 622−631.
(35) Domingos, R. F.; Baalousha, M. A.; Ju-Nam, Y.; Reid, M. M.; Tufenkji, N.; Lead, J. R.; Leppard, G. G.; Wilkinson, K. J. *Environ. Sci. Technol.* **2009**, *43*, 7277−7284.
(36) Han, X.; Kuang, Q.; Jin, M.; Xie, Z.; Zheng, L. *J. Am. Chem. Soc.* **2009**, *131*, 3152.
(37) Lynch, I.; Dawson, K. A. *Nano Today* **2008**, *3*, 40−47.
(38) Nel, A. E.; Madler, L.; Velegol, D.; Xia, T.; Hoek, E. M. V.; Somasundaran, P.; Klaessig, F.; Castranova, V.; Thompson, M. *Nat. Mater.* **2009**, *8*, 543−557.
(39) Shen, X. C.; Liou, X. Y.; Ye, L. P.; Liang, H.; Wang, Z. Y. *J. Colloid Interface Sci.* **2007**, *311*, 400−406.
(40) Zamaleeva, A. I.; Sharipova, I. R.; Porfireva, A. V.; Evtugyn, G. A.; Fakhrullin, R. F. *Langmuir* **2010**, *26*, 2671−2679.
(41) Nel, A.; Xia, T.; Meng, H.; Wang, X.; Lin, S.; Ji, Z.; Zhang, H. *Acc. Chem. Res.* **2013**, *46*, 607−621.
(42) Colvin, V. L. *Nat. Biotechnol.* **2003**, *21*, 1166−1170.
(43) Ivask, A.; Elbadawy, A.; Kaweeteerawat, C.; Boren, D.; Fischer, H.; Ji, Z.; Chang, C. H.; Liu, R.; Tolaymat, T.; Telesca, D.; Zink, J. I.; Cohen, Y.; Holden, P. A.; Godwin, H. A. *ACS Nano* **2014**, *8*, 374−386.
(44) Alito, C. L.; Gunsch, C. K. *Environ. Sci. Technol.* **2014**, *48*, 970−976.
(45) Agarwal, R.; Singh, V.; Jurney, P.; Shi, L.; Sreenivasan, S. V.; Roy, K. *Proc. Natl. Acad. Sci. U. S. A.* **2013**, *110*, 17247−17252.
(46) Untener, E. A.; Comfort, K. K.; Maurer, E. I.; Grabinski, C. M.; Comfort, D. A.; Hussain, S. M. *ACS Appl. Mater. Interfaces* **2013**, *5*, 8366−8373.
(47) Herd, H.; Daum, N.; Jones, A. T.; Huwer, H.; Ghandehari, H.; Lehr, C. M. *ACS Nano* **2013**, *7*, 1961−1973.
(48) Nativo, P.; Prior, I. A.; Brust, M. *ACS Nano* **2008**, *2*, 1639−1644.
(49) Klis, F. M.; Mol, P.; Hellingwerf, K.; Brul, S. *FEMS Microbiol. Rev.* **2002**, *26*, 239−256.
(50) Shaw, J. D.; Cummings, K. B.; Huyer, G.; Michaelis, M.; Wendland, B. Yeast as a Model System for Studying Endocytosis. *Exp. Cell Res.* **2001**, *271*, 1−9.
(51) Gref, R.; Minamitake, Y.; Peracchia, M. T.; et al. *Science* **1994**, *263*, 1600−1603.
(52) Otsuka, H.; Nagasaki, Y.; Kataoka, K. *Adv. Drug Delivery Rev.* **2012**, *64*, 246−255.
(53) Chen, R.; Huo, L.; Shi, X.; Bai, R.; Zhang, Z.; Zhao, Y.; Chang, Y.; Chen, C. *ACS Nano* **2014**, *8*, 2562−2574.
(54) Tsyusko, O. V.; Unrine, J. M.; Spurgeon, D.; Blalock, E.; Starnes, D.; Tseng, M.; Joice, G.; Bertsch, P. M. *Environ. Sci. Technol.* **2012**, *46*, 4115−4124.
(55) Gardarin, A.; Chédin, S.; Lagniel, G.; Aude, J. C.; Godat, E.; Catty, P.; Labarre, J. *Mol. Microbiol.* **2010**, *76*, 1034−1048.
(56) Cox, J. S.; Walter, P. *Cell* **1996**, *87*, 391−404.
(57) Xiong, S.; Xi, B.; Qian, Y. *J. Phys. Chem. C* **2010**, *114*, 14029−14035.
(58) Chen, P.; Powell, B. A.; Mortimer, M.; Ke, P. C. *Environ. Sci. Technol.* **2012**, *46*, 12178−12185.
(59) Chen, W.; Duan, L.; Zhu, D. Q. *Environ. Sci. Technol.* **2007**, *41*, 8295−8300.
(60) Scrimale, T.; Didone, L.; de Mesy Bentley, K.; Krysan, D. *Mol. Biol. Cell* **2009**, *20*, 164−175.
(61) Plumb, R.; Zhang, Z.; Appathurai, S.; Mariappanf, M. *eLife* **2015**, *4*, e07426.
(62) Yu, Q.; Wang, H.; Xu, N.; Cheng, X.; Wang, Y.; Zhang, B.; Xing, L.; Li, M. *Microbiology* **2012**, *158*, 2272−2282.

DOI: 10.1021/acs.nanolett.5b04487
Nano Lett. 2016, 16, 688−694